Electronic Supplementary Information (ESI)

Rational design of ZIF-derived nanocarbon with dual metal active sites via molten salt strategy for advancing oxygen electrocatalysis

Sakshi Bhardwaj[a], Tribani Boruah[a], and Ramendra Sundar Dey[a]*

[a]*Institute of Nano Science and Technology, Sector-81, Mohali, 140306, Punjab, India*

**Corresponding author. E-mail: rsdey@inst.ac.in*

Table of contents

1. Instrumentation

A Bruker AXS D-8 Advanced SWAX diffractometer was employed to obtained the powder X-diffration (PXRD) pattern via utilising Cu-Kα(λ= 1.5406 Å) source of radiation. The Fourier-transform infrared spectroscopy (FTIR) technique was used to analyze the bonding connectivity of the as-synthesized material using a Perkin Elmer Spectrum 100 spectrophotometer. Further to confirm the presences of different types N, O, C XPS analysis has been performed using Thermo Fisher Instrument with Cu-kα as source of radiation. While, BET surface area analysis data were obtained from a surface area/porosity analyzer (Quantachrome Autosorb-iQ, USA). Additionally, to determine the pore size distribution of the generated N_2 adsorption-isotherm, Non-Local Density Functional Theory (NLDFT) was utilized. Moreover, to determine the thermal stability of the as-synthesized material, Thermo-gravimetric analysis was carried out in a Mettler Toledo TGA/DTA 851e TA-SDT Q-600 instrument. Field emission scanning electron microscopy (FESEM) images of the material were collected from a JEOL JEM 6700 instrument. Transmission electron microscopy (TEM) images were taken using JEOL JEM 2100 and high-resolution images were obtained using scanning tunneling microscope (STM) from Nanosurf NaioSTM.

2. Electrochemical measurements:

CHI 760E and Metrohm Multi Auto-lab/M204 electrochemical work-station consisting of three-electrode cell namely working electrode [RDE (rotating disk electrode) dia-3mm, RRDE (rotating ring disk electrode) dia-5mm], reference electrode (3M-KCl, Ag/AgCl) and counter electrode (graphite rod dia-10 mm) was used to record the electrochemical data for the as-synthesized porous polymeric network. The catalyst ink

was prepared by using 5 mg of catalyst in water and isopropanol (1:1) and sonicating for 30 minutes. For comparison, Pt/C ink was prepared in ethanol and DI water containing Nafion (5%) solution, which was dispersed by ultrasonication for 30 min. Before drop-casting, the catalyst on the electrodes, the glassy carbon, RDE, and RRDE electrodes were polished by using 1, 0.3, and 0.05 μm alumina powder (Al_2O_3) and washed with DI water ultrasonically. All the catalysts were drop-casted on the electrodes to maintain a mass loading of 0.65 mg cm^{-2}. Moreover, the following experiments have been performed after 30 minutes of oxygen gas purging in 0.1 M KOH to record the cyclic voltammetry (CV), llinear sweep voltammetry (LSV), chronoamperometry, and electrochemical impedance spectroscopy (EIS), respectively.

The obtained potentials were calibrated to RHE (reversible hydrogen electrode) using the equation given below.[3]

$$E(RHE)\ (V) = E\_(Ag/AgCl)\ \ (3\ M\ KCl)\ V + \ (0.058\ \times\ pH)\ \ V + \ 0.210\ V \qquad (S1)$$

The number of electron transfer (n) per O_2 participate in ORR can be determined by Koutecky-Levich (K-L) equation-

$$\frac{1}{J} = \frac{1}{JL} + \frac{1}{JK} = \frac{1}{B\omega^{\frac{1}{2}}} + \frac{1}{J\mathbf{K}} \qquad (S2)$$

J is the measured current density, J_K (kinetic current density) and J_L (diffusion-limiting current density), ω is the angular velocity of the disk (ω = 2πN, linear rotation speed (N), n is the overall number of electrons transferred in ORR, Faraday constant (F = 96485 C mol^{-1}), ϑ is the kinematic viscosity of the electrolyte, C_0 is the bulk concentration of O_2, k is the electron transfer rate constant diffusion coefficient, and (D_0) of O_2 in electrolyte solution. The *B* and J_K values can be resolved from the Koutecky-Levich (K-L) plots based on the Levich equation below.

$$B = 0.62nFC\mathbf{0}\ D\mathbf{0}^{2/3}\vartheta^{-1/6} \qquad (S3)$$

$$J\mathrm{K}\ =\ \mathrm{nFk}C0 \qquad (S4)$$

For the ORR analysis, the total no. of electrons (n) participating in the reaction was calculated by using equation (5) while, the percentage of hydrogen peroxide ($\%H_2O_2$) generation was evaluated by using equation (6),

$$n = 4 \times \frac{I\mathbf{D}}{I\mathbf{D} + \frac{I\mathbf{R}}{N}} \qquad (S5)$$

$$\%H\mathbf{2}O\mathbf{2} = \mathbf{200} \times \frac{\frac{I\mathbf{R}}{N}}{\frac{I\mathbf{R}}{N} + I\mathbf{D}} \qquad (S6)$$

3. Supplementary Figures

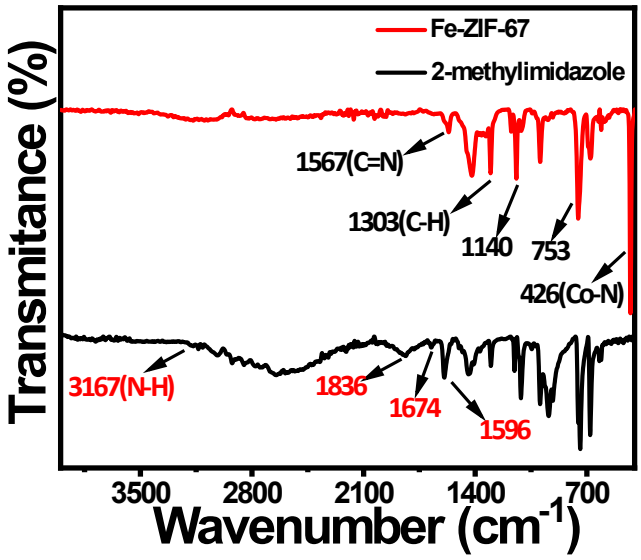

Fig. S1. FTIR spectra of Fe-ZIF-67 and precursor 2-methylmethylimidazol.

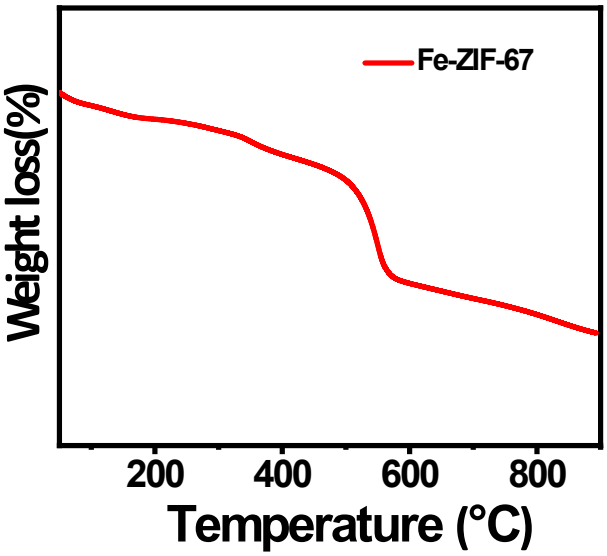

Fig. S2. Thermogravimetric analysis (TGA) of as synthesized material Fe-ZIF-67.

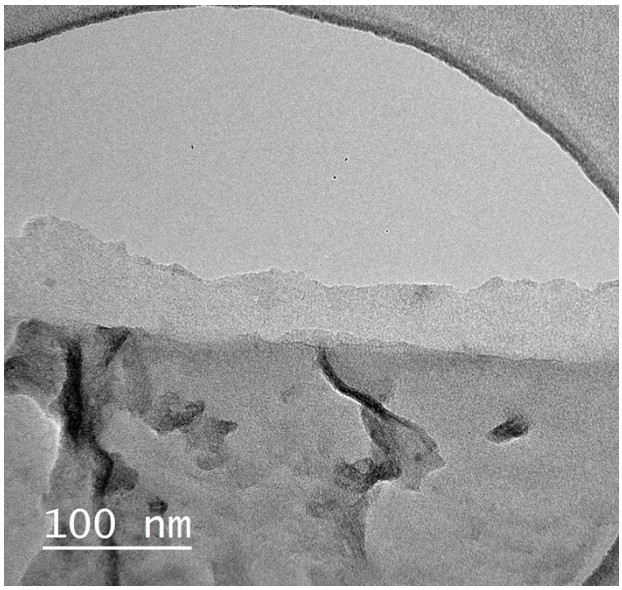

Fig. S3. TEM image of Fe,Co-HPNC.

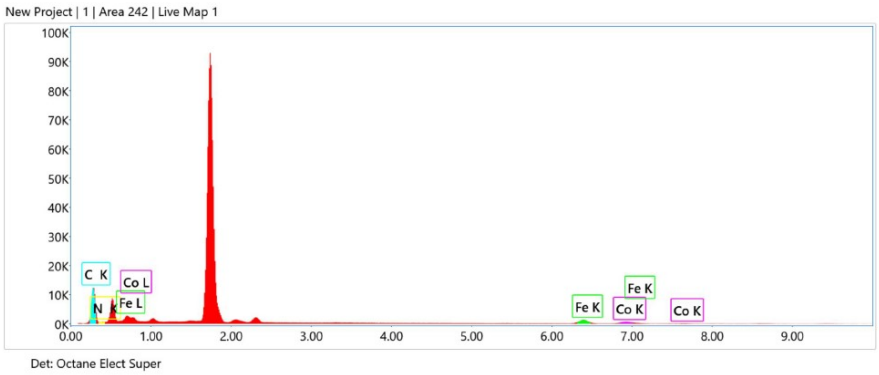

Fig. S4. EDX analysis of Fe, Co-HPNC catalyst.

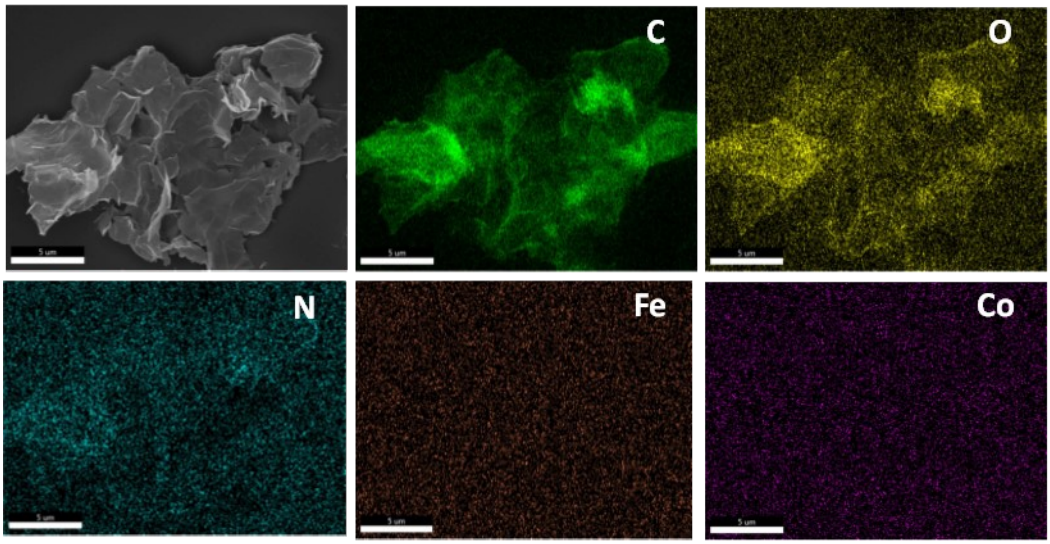

Fig. S5. EDX mapping of Fe, Co-HPNC catalyst.

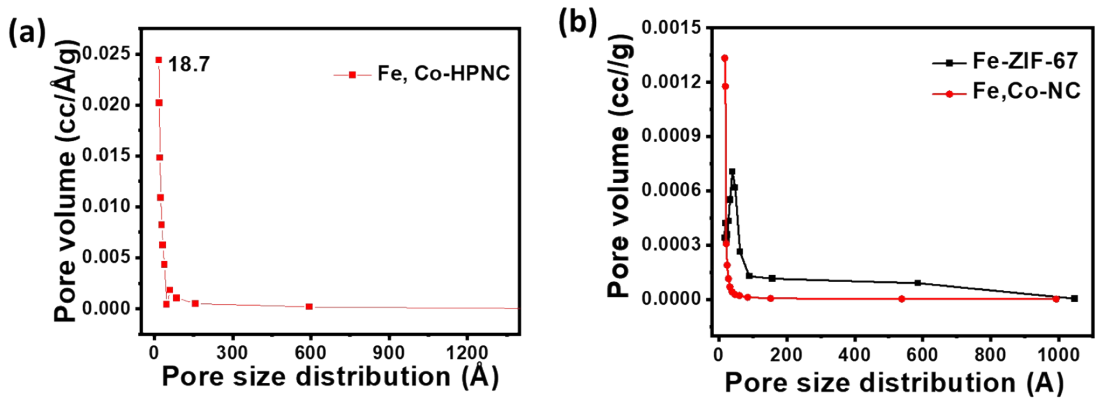

Fig. S6. Pore size distribution curve of synthesized material (a) Fe, Co-HPNC, (b) Fe-ZIF-67 and Fe, Co-NC.

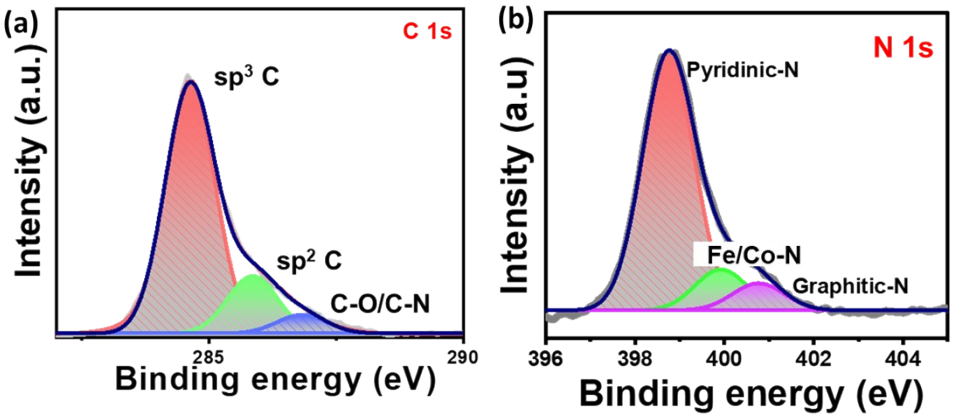

Fig. S7. High resolution deconvoluted XPS spectra of (a) C 1s, (b) N 1s of Fe, Co-HPNC.

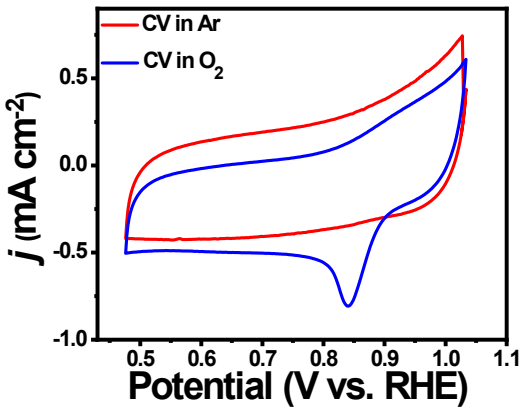

Fig. S8. CV plots of Fe, Co-HPNC in 0.1 M KOH saturated with Ar and O_2 at 10 mV s^{-1} scan rate.

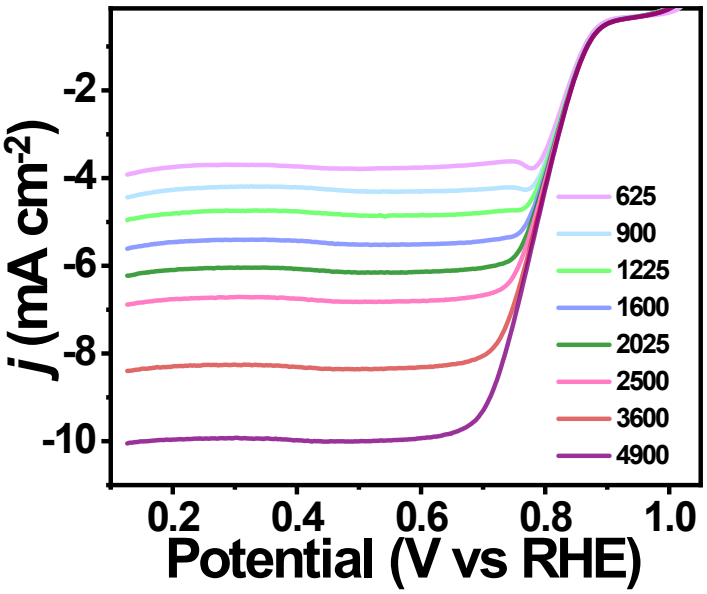

Fig. S9. (a) LSV curve of Fe, Co-HPNC at different rotations from (625-4900) using RRDE in 0.1 M KOH.

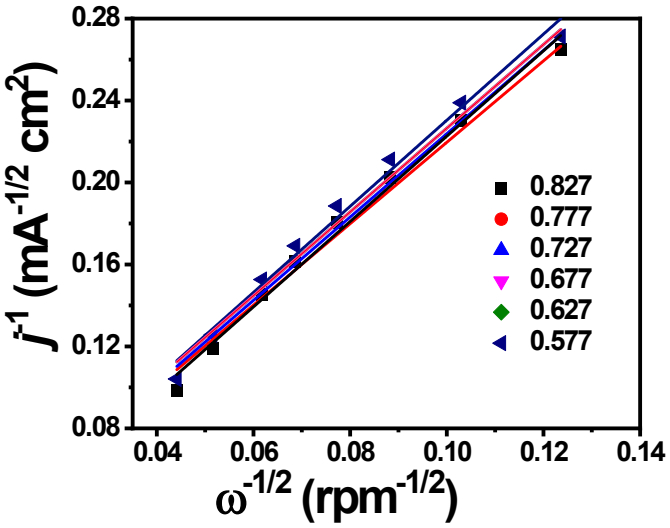

Fig. S10. (a) KL-plot corresponding to LSV curve at different rotations of Fe, Co-HPNC.

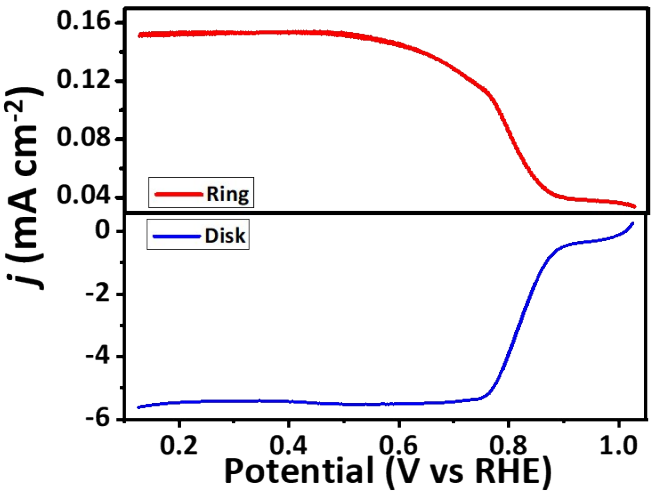

Fig. S11. Ring and disk current of Fe, Co-HPNC catalyst in O_2 saturated 0.1 M KOH at 1600 rpm.

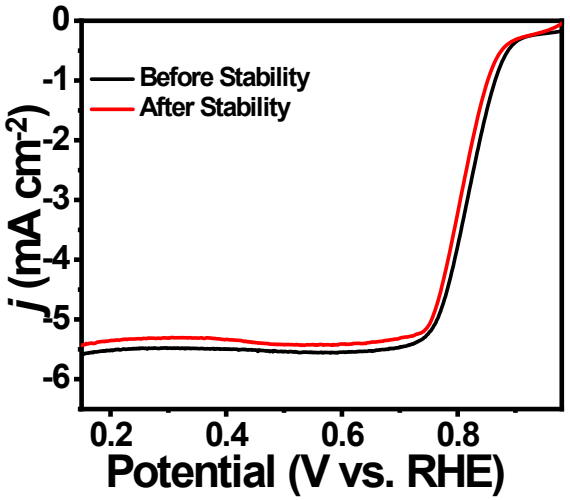

Fig. S12. LSV of Fe, Co-HPNC taken before and after stability in O_2 saturated 0.1 M KOH at 1600 rpm.

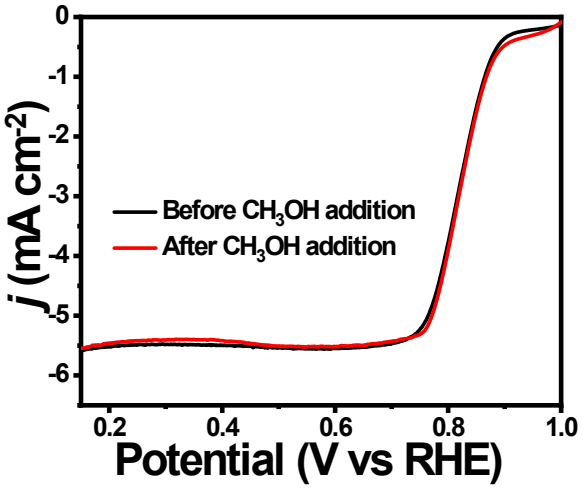

Fig. S13. LSV of Fe, Co-HPNC taken before and after methanol tolerance in O_2 saturated 0.1 M KOH at 1600 rpm.

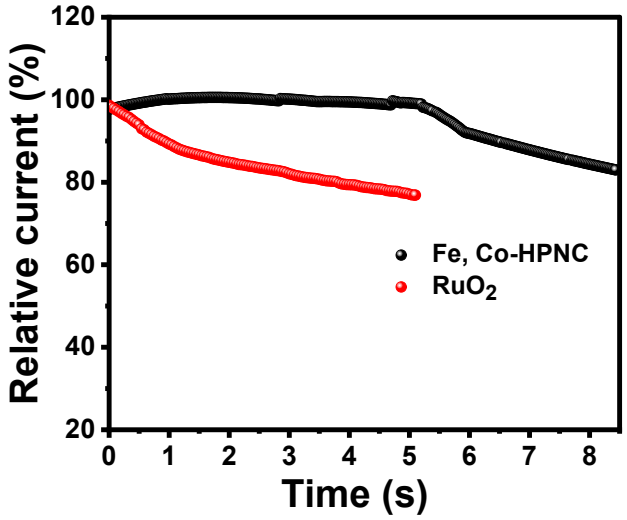

Fig. S14. Chronoamperometric response of Fe, Co-HPNC taken in 1.0 M KOH for OER stability.

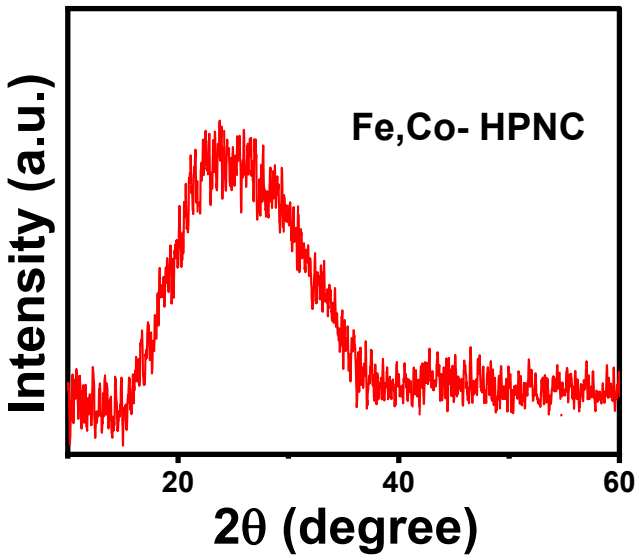

Fig. S15. XRD pattern of Fe, Co-HPNC taken after stability.

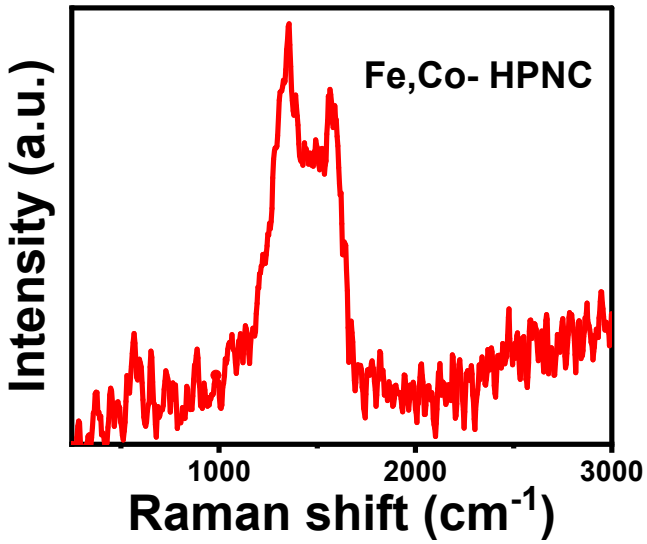

Fig. S16. Raman spectra of Fe, Co-HPNC taken after stability.

Table S1. BET surface area and total pore volume of synthesized material Fe-ZIF-67, Fe, Co-NC and Fe, Co-HPNC.

Catalyst	BET Surface Area(S_{BET})	Total Pore Volume(cc/g)
Fe-ZIF-67	131.57	0.064
Fe,Co-NC	836.8	0.415
Fe, Co-HPNC	1758	1.33

Table S2. Comparison table of ΔE of various catalysts in literature with Fe, Co-HPNC.

Catalysts	Electrolyte	OCV E (V)	E(1/2) (V) vs RHE	Peak power density (mW cm-2)	E$_{j10}$ (V) vs RHE	ΔE (V)	Ref.	Ref.
Fe,Co-HPNC	0.1 M KOH for ORR, and N2 saturated 1 M KOH for OER.	1.42	0.86	216	1.57	0.7	Current work	
FeCo@MNC	0.1M KOH	1.51	0.901	311.2	1.596	0.695	1	1
FeCo-N-3D-HG	0.1M KOH	1.46	0.860	238.6	1.62	0.760	2	2
Fe3Co7-NC	0.1M KOH	1.51	0.893	133	1.57	0.677	3	3
Fe,Co,N-C	0.1M KOH	1.40	0.90	198.4	1.64	0.74	4	4
Meso/micro-FeCo−N/C	0.1M KOH	1.4	0.84	150	1.60	0.77	7	5
Fe-Co$_4$N@N-C	0.1M KOH		0.83		1.55	0.72		6
Meso/micro-FeCoNx-CN-30	0.1 M KOH for ORR, and N2 saturated 1 M KOH for OER.		0.886		1.67	0.784		7
Fe1.2Co@NC/NCNTs	0.1M KOH		0.82		1.585	0.765		8
FeCo@NCNS	0.1 M KOH		0.827		1.597	0.772		9
FeCo/N-DNC	0.1M KOH		0.81		1.62	0.81		10
FeCo-NCps	0.1M KOH		0.845		1.61	0.76		11
CoFe/N-GCT	0.1M KOH		0.79		1.67	0.88		12
N-GCNT/FeCo-3	0.1M KOH		0.92		1.73	0.81		13
(Fe,Co)SPPc	O2 saturated 0.1 M KOH for ORR, and O2 saturated 1 M KOH for OER.		0.830		1.583	0.753		14
FeCo-NCNFs-800	0.1M KOH		0.817		1.686	0.869		15
CMP-CoFe/C	0.1M KOH		0.84		1.64	0.88		16

Note: CoFe/N-GCT: CoFe alloy nanoparticles embedded in N-doped bamboo-like CNTs tangled with reduced graphene oxide (rGO) nanosheets; CNS: porous carbon nanosheets; NCNTs: N-doped carbon nanotubes; N-GCNT: N-doped graphitic carbon nanotubes; NPC: porous carbon nanosheets; CMP: conjugated microporous polymers; SPPc: silica-protected Fe- and Co-modified, S-containing polyphthalocyanine; ps: peanut shell

Table S3. Comparison of electrochemical activity of Fe,Co-HPNC in metal-air battery with reported catalysts:

Fe1.2Co@NC/ NCNTs	0.765	1.43	194	[8]
FeCo/N-DNC	0.81	1.43	115	[10]
FeCo-NCps	0.76	1.43	242	[11]
CoFe/N-GCT	0.88	1.43	203	[12]
N-GCNT/FeCo-3	0.81	1.48	89.3	[13]
(Fe,Co)SPPc	0.753	1.47	158.6	[14]
FeCo-NCNFs-800	0.869	1.48	74	[15]

References:

(1) Fan, M.; Liu, P.; Cheng, Y.; Tang, H.; Jin, B.; Zhang, H. Fe-N4/Co-N4 Active Sites Engineered Porous Carbon with Encapsulated FeCo Alloy as an Efficient Bifunctional Catalyst for Rechargeable Zinc-Air Battery. *J Alloys Compd* **2023**, *935*, 168107. https://doi.org/10.1016/J.JALLCOM.2022.168107.

(2) Ji, C.; Zhang, T.; Sun, P.; Li, P.; Wang, J.; Zhang, L.; Sun, Y.; Duan, W.; Li, Z. Facile Preparation and Properties of High Nitrogen-Containing Fe/Co/N Co-Doped Three-Dimensional Graphene Bifunctional Oxygen Catalysts for Zinc Air Battery. *Int J Hydrogen Energy* **2023**, *48* (67), 26328–26340. https://doi.org/10.1016/J.IJHYDENE.2023.03.333.

(3) Gu, T.; Zhang, D.; Yang, Y.; Peng, C.; Xue, D.; Zhi, C.; Zhu, M.; Liu, J.; Gu, T.; Yang, Y.; Zhu, M.; Liu, J.; Zhang, D.; Peng, C.; Xue, D.; Zhi, C. Dual-Sites Coordination Engineering of Single Atom Catalysts for Full-Temperature Adaptive Flexible Ultralong-Life Solid-State Zn−Air Batteries. *Adv Funct Mater* **2023**, *33* (8), 2212299. https://doi.org/10.1002/ADFM.202212299.

(4) Sarkar, S.; Biswas, A.; Siddharthan, E. E.; Thapa, R.; Dey, R. S. Strategic Modulation of Target-Specific Isolated Fe,Co Single-Atom Active Sites for Oxygen Electrocatalysis Impacting High Power Zn-Air Battery. *ACS Nano* **2022**, *16*, 7890–7903. https://doi.org/10.1021/ACSNANO.2C00547/SUPPL_FILE/NN2C00547_SI_002.MP4.

(5) Shui, H.; Jin, T.; Hu, J.; Liu, H. In Situ Incorporation Strategy for Bimetallic FeCo-Doped Carbon as Highly Efficient Bifunctional Oxygen Electrocatalysts. *ChemElectroChem* **2018**, *5* (10), 1401–1406. https://doi.org/10.1002/CELC.201800013.

(6) Xu, Q.; Jiang, H.; Li, Y.; Liang, D.; Hu, Y.; Li, C. In-Situ Enriching Active Sites on Co-Doped Fe-Co4N@N-C Nanosheet Array as Air Cathode for Flexible Rechargeable Zn-Air Batteries. *Appl Catal B* **2019**, *256*, 117893. https://doi.org/10.1016/J.APCATB.2019.117893.

(7) Li, S.; Cheng, C.; Zhao, X.; Schmidt, J.; Thomas, A. Active Salt/Silica-Templated 2D Mesoporous FeCo-Nx-Carbon as Bifunctional Oxygen Electrodes for Zinc–Air Batteries. *Angewandte Chemie International Edition* **2018**, *57* (7), 1856–1862. https://doi.org/10.1002/ANIE.201710852.

(8) Li, S.; Chen, W.; Pan, H.; Cao, Y.; Jiang, Z.; Tian, X.; Hao, X.; Maiyalagan, T.; Jiang, Z. J. FeCo Alloy Nanoparticles Coated by an Ultrathin N-Doped Carbon Layer and Encapsulated in Carbon Nanotubes as a Highly Efficient Bifunctional Air Electrode for Rechargeable Zn-Air Batteries. *ACS Sustain Chem Eng* **2019**, *7* (9), 8530–8541.

https://doi.org/10.1021/ACSSUSCHEMENG.9B00307/ASSET/IMAGES/LARGE/SC-2019-00307G_0007.JPEG.

(9) Liu, T.; Cai, S.; Gao, Z.; Liu, S.; Li, H.; Chen, L.; Li, M.; Guo, H. Facile Synthesis of the Porous FeCo@nitrogen-Doped Carbon Nanosheets as Bifunctional Oxygen Electrocatalysts. *Electrochim Acta* **2020**, *335*, 135647. https://doi.org/10.1016/J.ELECTACTA.2020.135647.

(10) Fu, G.; Liu, Y.; Chen, Y.; Tang, Y.; Goodenough, J. B.; Lee, J. M. Robust N-Doped Carbon Aerogels Strongly Coupled with Iron–Cobalt Particles as Efficient Bifunctional Catalysts for Rechargeable Zn–Air Batteries. *Nanoscale* **2018**, *10* (42), 19937–19944. https://doi.org/10.1039/C8NR05812A.

(11) Liu, J.; He, T.; Wang, Q.; Zhou, Z.; Zhang, Y.; Wu, H.; Li, Q.; Zheng, J.; Sun, Z.; Lei, Y.; Ma, J.; Zhang, Y. Confining Ultrasmall Bimetallic Alloys in Porous N–Carbon for Use as Scalable and Sustainable Electrocatalysts for Rechargeable Zn–Air Batteries. *J Mater Chem A Mater* **2019**, *7* (20), 12451–12456. https://doi.org/10.1039/C9TA02264C.

(12) Liu, X.; Wang, L.; Yu, P.; Tian, C.; Sun, F.; Ma, J.; Li, W.; Fu, H. A Stable Bifunctional Catalyst for Rechargeable Zinc–Air Batteries: Iron–Cobalt Nanoparticles Embedded in a Nitrogen-Doped 3D Carbon Matrix. *Angewandte Chemie International Edition* **2018**, *57* (49), 16166–16170. https://doi.org/10.1002/ANIE.201809009.

(13) Su, C. Y.; Cheng, H.; Li, W.; Liu, Z. Q.; Li, N.; Hou, Z.; Bai, F. Q.; Zhang, H. X.; Ma, T. Y. Atomic Modulation of FeCo–Nitrogen–Carbon Bifunctional Oxygen Electrodes for Rechargeable and Flexible All-Solid-State Zinc–Air Battery. *Adv Energy Mater* **2017**, *7* (13), 1602420. https://doi.org/10.1002/AENM.201602420.

(14) Chen, L.; Cui, L. L.; Wang, Z.; He, X.; Zhang, W.; Asefa, T. Co8FeS8/N,S-Doped Carbons Derived from Fe-Co/S-Bridged Polyphthalocyanine: Efficient Dual-Function Air-Electrode Catalysts for Rechargeable Zn-Air Batteries. *ACS Sustain Chem Eng* **2020**, *8* (35), 13147–13158. https://doi.org/10.1021/ACSSUSCHEMENG.0C00124/ASSET/IMAGES/LARGE/SC0C00124_0007.JPEG.

(15) Yang, L.; Feng, S.; Xu, G.; Wei, B.; Zhang, L. Electrospun MOF-Based FeCo Nanoparticles Embedded in Nitrogen-Doped Mesoporous Carbon Nanofibers as an Efficient Bifunctional Catalyst for Oxygen Reduction and Oxygen Evolution Reactions in Zinc-Air Batteries. *ACS Sustain Chem Eng* **2019**, *7* (5), 5462–5475. https://doi.org/10.1021/ACSSUSCHEMENG.8B06624/ASSET/IMAGES/LARGE/SC-2018-066242_0011.JPEG.

(16) Li, H.; Sui, Z. An in Situ Coupling Strategy for the Preparation of Heterometal-Doped Carbon Frameworks as Efficient Bifunctional ORR/OER Electrocatalysts. *New Journal of Chemistry* **2019**, *43* (46), 17963–17973. https://doi.org/10.1039/C9NJ04422A.